Available online at www.sciencedirect.com
ScienceDirect
Tectonophysics 426 (2006) 239–251
TECTONOPHYSICS
www.elsevier.com/locate/tecto

End effects on stress dependent permeability measurements

R.I. Korsnes *, R. Risnes, I. Faldaas, T. Norland

Stavanger University College, P.O. Box 8002, N-4068 Stavanger, Norway

Accepted 7 February 2006
Available online 30 June 2006

Abstract

Permeability changes have been studied under deviatoric stresses for chalk cores and under both hydrostatic- and deviatoric stresses for sandstone cores at room temperature. To avoid end effects in the triaxial cell, caused by friction between the axial steel pistons and the sample, the cell was modified to have pressure outlets from the mid-section of the sample with pressure tubes connected to the outside of the cell for pressure recording. Both permeabilities over the mid-section and over the total core were determined during the action of stresses. The chalk cores with permeability in the range of $1–3\times10^{-15}$ m^2 and porosity of about 40–45% were flooded with methanol, while the sandstone cores with permeability values varying from 8 to 100×10^{-15} m^2 and porosity of about 30% were flooded with a mineral oil. Major observations were:

(1) For the chalk cores, 4 out of 8 samples showed a mid-section permeability with a factor of 1.2 to 1.4 higher than the overall permeability, the remaining 4 samples did not show differences in permeability values taking into account the error on measurements.
(2) For the sandstone samples, the mid-section permeability was a factor of 1.2 to 2.4 higher than the overall permeability.
(3) In all cases during the deviatoric phase, the change in permeability was rather small, even if the tests were run beyond the yield point.
(4) The permeability generally decreased with increasing hydrostatic stresses.

Keywords: Permeability; Stress; End effects; Chalk; Sandstone

1. Introduction

It is reported in the literature that the permeability of porous media generally decreases with increasing effective stresses, but the permeability measurements can be performed under different stress conditions: hydrostatic and non-hydrostatic stress conditions. In a hydrostatic test, the axial stress is equal to the confining stress. Non-hydrostatic tests can for example be triaxial compression tests or constant stress ratio, K, tests. The triaxial compression test consists of two phases, first a hydrostatic phase and then a deviatoric phase. In the deviatoric phase, the confining pressure is kept constant, and the axial stress or loading is increased until failure or beyond. Constant stress ratio tests are compression tests where the ratio between the confining pressure and the axial stress, K value, are kept constant. K-ratio equal to 0 corresponds to an uniaxial compression test, which is a test with zero confining pressure, while a K-ratio equal to 1 represents a hydrostatic test. David et al. (1994) investigated the dependence of permeability on hydrostatic stresses on five sandstones with porosities ranging from 14% to 35% and showed a permeability decrease up to 3 orders of magnitude. The permeability evolution in

* Corresponding author.
E-mail address: reidar.i.korsnes@uis.no (R.I. Korsnes).

0040-1951/$ - see front matter © 2006 Elsevier B.V. All rights reserved.
doi:10.1016/j.tecto.2006.02.020

Table 1
Chalk properties

Chalk type	Liège	Aalborg
Age	Upper Campanian	Upper Cretaceous
Porosity	Approx. 40%	Approx. 45%
Silica content	<2%	Approx. 4%
Permeability	$1–2\times10^{-15}$ m^2	$3–5\times10^{-15}$ m^2

sandstone is, however, sensitive to the stress path. In triaxial compression tests, non-hydrostatic stresses were also found to cause a permeability reduction as long as the shear stress was below yield level, but the permeability decreased more rapidly when the shear stress exceeded the yield level (Holt, 1989; Zhu and Wong, 1997). Another study by Rhett and Teufel (1992) on the effect of reservoir stress path on sandstone permeability showed an increase in permeability when values of constant stress ratio were below 0.75. Thus, depending on the stress path followed, both increases and decreases in permeability could be detected. Few studies on stress dependent permeability have been reported on chalk. Teufel and Warpinski (1990) performed hydrostatic tests on chalk samples with porosities of 24% and 36%, and the decrease in permeability was observed to be less than 15% when the confining stress was increased from 6.9 MPa to 55.2 MPa. Teufel and Rhett (1992) studied the effect of reservoir stress on permeability of fractured chalk, and during pore pressure drawdown they observed a smaller reduction in fracture permeability when constant stress ratios became smaller.

The permeability measurements can be influenced by the laboratory test method used. Obviously, permeability studies without external stress will be different from measurements under hydrostatic loading. In most cases, the changes in permeability have been determined using the overall pressure drop over the core. In-situ stress conditions may be approached in a triaxial cell, but the friction between the axial pistons and the sample may cause stress concentrations, and thereby a non-homogeneous strain pattern towards the sample ends. Thus, it could be argued that the laboratory results of this type of measurements are not necessarily applicable to in-situ conditions.

The scope of the present paper is to study end effects in permeability measurements under stress. The basic idea behind the modified test procedure was to determine the pressure gradient over the mid-section of the sample. Permeability measurements from the mid-section were compared with measurements using the differential pressure over the total core length.

2. Experimental

2.1. Materials

The high porosity outcrop chalk samples came from two different quarries, i.e. Lixhe near Liège in Belgium and Roerdal near Aalborg in Denmark. The mechanical properties of Liège and Aalborg chalk are quite similar. Aalborg chalk has in general somewhat higher porosity values, and it also has higher silica content. The main characteristics of these chalks before testing are given in Table 1. In order to obtain comparable samples, each of the cores was drilled from the same chalk block with an oversized core bit using circulating water for cooling. The samples were then dried for 24 h at a temperature of 110–120 °C and finally shaped in a lathe to the correct size, diameter of 37 mm and length of about 85 mm, Table 2.

Sandstone reservoir cores were received from Statoil and used without further treatments.

Methanol (purity >99%, viscosity 0.547×10^{-3} Pa s at 25 °C and density 790 kg/m^3 at 20 °C) and mineral oil (EDC 99DW, viscosity $4.7\times10^{-}3$ Pa s at 20 °C and density of 811.4 kg/m^3 at 15 °C) were used as flooding fluids for chalk and sandstone, respectively.

2.2. Core preparation/treatments

After shaping the samples to the correct size, the cores were dried under vacuum (less than 4–5 Pa) for 12 h before the saturating fluid was introduced. The samples were then stored in the respective fluids until the tests were performed. In order to avoid a large pressure drop over the

Table 2
Chalk sample data

Sample no.	Diameter (mm)	Length (mm)	Dry weight (g)	Saturated weight (g)	Bulk volume (mm^3)	Pore volume (mm^3)	Porosity (%)
Al1	37.0	85.9	137.96	169.04	92.4	39.3	42.6
Al4	37.0	85.7	135.01	168.85	92.2	42.8	46.5
Al5	37.0	85.7	135.50	169.10	92.2	42.5	46.2
Al7	37.0	85.8	134.36	166.67	92.3	40.9	44.3
Li1	37.0	85.2	147.19	177.50	91.6	38.4	41.9
Li2	37.0	85.7	148.73	178.30	92.2	37.4	40.6
Li3	37.0	85.9	148.92	179.14	92.4	38.3	41.4
Li5	36.8	85.8	145.47	174.40	91.3	36.6	40.1

Table 3
Sampling data for the sandstone cores

Seal peels		Core samples		
No.	Depth	No.	Depth (m)	Direction
1	1448.50–1449.00	1	1448.85	Horizontal
		2	1448.95A	Vertical
		3	1448.95B	Vertical

samples during flooding, methanol was used as a saturating fluid for the low permeability chalk samples due to its low viscosity.

The porosity of the chalk samples was determined from the dimensions and the weight of dry and saturated material. The porosity values varied within a few percent, even for samples taken from the same block, Table 2. The porosity was mainly measured in order to eliminate non-typical plugs (Da-Silva et al., 1985).

The received sandstone core samples had been tested, shaped and dried prior to delivery to the laboratory. The sampling depth and the sampling direction (vertical or horizontal) for the individual cores are listed in Table 3. The samples arrived in an apparently "dry" state. Before saturation with mineral oil, the samples were dried overnight under vacuum. The porosity of the samples was calculated in two different ways. Based on dry weight, the solid volume was calculated by assuming a grain density of 2.65 g/cm^3, which was reported by Statoil. The corresponding porosity is referred to as dry porosity. Alternatively, the volume of mineral oil in the pores determined the porosity after saturation. This porosity value is referred to as the saturated porosity, Table 4.

2.3. Equipment

The cell used for the permeability measurements is basically a hydraulically operated standard triaxial test cell. The cell is operated by 3 high-pressure pumps to control: confining pressure, axial pressure and fluid circulation. The piston system of the cell is compensated so that the confining pressure is applied also in the axial direction. The pump in the axial circuit will thus provide only the additional pressure needed. The cell is not equipped for measuring lateral displacement; however the axial displacement is measured by an outside LVDT (±0.05 mm) that follows the movement of the piston. An inconvenience of this set-up is that the axial displacement cannot be measured in pure hydrostatic tests. To keep the piston in contact with the sample, some pressure must be applied in the axial circuit. Thus, the axial stress will always be slightly higher than the confining stress as an alternative to pure hydrostatic tests in the cell. The pressure limit of the pumps is 60 MPa.

Two different pressure transducers were used with pressure limits of 62 and 249 kPa, with an accuracy of 0.075% of span. The largest pressure transducer, 249 kPa, was used to measure the differential pressure over the entire sample, and the small pressure transducer was used to measure the differential pressure over the mid-section of the sample.

To allow pressure recordings from the mid-section of the sample, the sleeve was prepared with pressure tubes, which were connected to the exterior of the cell. The sleeves for the permeability tests were prepared from a two component silicon rubber (Rhodorsil A+B), poured into a mould where the pressure outlet tubes could be held in a fixed position. The distance between the pressure outlet openings was 40 mm. The sleeve thickness was 5 mm, and the pressure tubes were 1/16 in. steel tubes equipped with a small flange towards the sample to assure sealing when the sleeve is compressed under the confining pressure. A schematic illustration and a picture are shown in Fig. 1.

Table 4
Sandstone core data

No.	Diameter (mm)	Length (mm)	Volume (cm^3)	Initial weight (g)	Dry weight (g)	Saturated weight (g)	Dry porosity (%)[a]	Saturated porosity (%)[b]
1	37.8	85.8	96.2	182.33	173.67	198.70	31.9	31.2
2	38.0	86.5	98.1	185.07	177.10	199.62	31.9	27.6
3	38.0	83.6	94.8	182.88	174.63	192.34	30.5	22.4

[a] Based on the bulk volume and mineral density of 2.65 g/cm^3.
[b] Saturated with mineral oil.

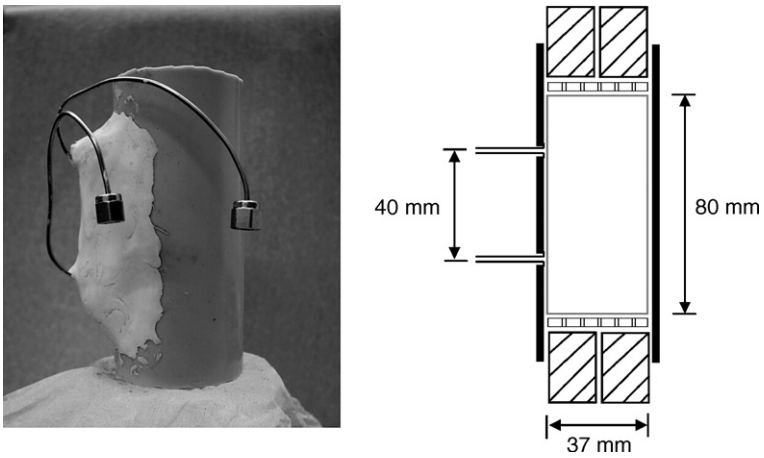

Fig. 1. Picture and schematic illustration of the modified test sleeve.

2.4. Test procedure

When placing the core in the sleeve, a circular filter paper was placed at the sample ends to retain any fines produced in the test in order to avoid filling up or plugging of the circulating tubes. Additionally, perforated steel discs were installed to distribute the fluid flow into the sample. Blind tests with a hollow cylinder steel sample showed that the pressure drop over the discs and the connecting tubes was negligible at the flow rates used in the later experiments. The cores were always placed in a vertical direction, and the circulating fluid was flooded upwards. Care was taken to avoid air bubbles in the connecting tubes. The flow rates were programmed from a pump with flow rates ranging from 0.01 to 10 ml/min with accuracy $<\pm 1\%$ and repeatability $<1\%$. The low permeability chalk samples were flooded with flow rates of 0.05 and 0.3 ml/min, and the flow rate varied between 0.025 ans 0.1 ml/min for the sandstone samples depending on the permeability. To compensate for evaporation, 1% was added to the flow rate uncertainties.

The stress paths to be followed for the chalk tests are illustrated in Fig. 2, where the yield envelope for methanol saturated chalk was based on data from Risnes (2001).

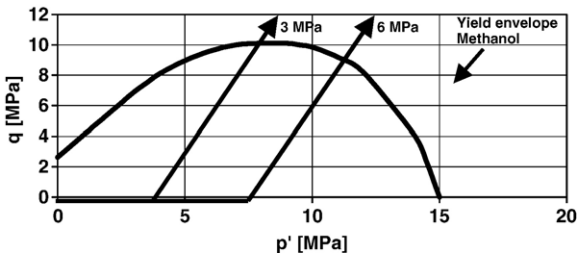

Fig. 2. Stress path for permeability tests with chalk samples.

The yield curve in Fig. 1 is presented in a q–p' diagram, which is a convenient plot to use for materials where failure mechanisms other than shear failure become important. Generalized shear stress q is defined by:

$$q = \frac{1}{\sqrt{2}}\sqrt{(\sigma_1'-\sigma_2')^2 + (\sigma_2'-\sigma_3')^2 + (\sigma_1'-\sigma_2')^2} \qquad (1)$$

which reduces to the stress difference for tests on cylindrical samples where two of the principal stresses are equal. The prime mark, σ', denotes effective stress, but in the formula for q, only stress differences appear, and total stresses could be used as well. The average effective stress p' is given by:

$$p' = \frac{1}{3}(\sigma_1' + \sigma_2' + \sigma_3') \qquad (2)$$

The tests were performed in a triaxial cell with confining pressure of 3 and 6 MPa, followed by a deviatoric

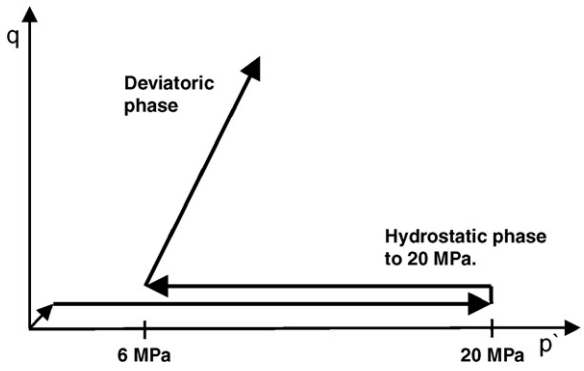

Fig. 3. Stress path for permeability tests with sandstone samples.

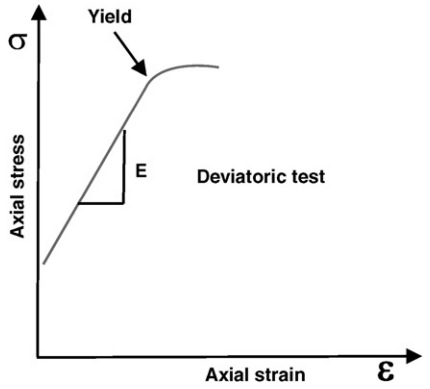

Fig. 4. Typical deviatoric stress–strain plot for the chalk cores.

phase beyond yield. The axial loading was run in steps of 0.5, 1.0, 2.0, 3.0, 4.0, 5.0, 6.0 and 7.0 MPa. Axial loading was stopped at every loading step, and the stresses were kept constant while measuring the differential pressure.

The stress path followed for the sandstone samples was: (1) hydrostatic loading to 20 MPa; (2) hydrostatic unloading to 6 MPa; (3) deviatoric loading until failure with 6 MPa confining pressure. The hydrostatic loading and unloading was run in steps of 2.0 MPa, and it ended before hydrostatic yield and stopped between 18 and 20 MPa. The deviatoric phase was also run with axial loading steps of 2.0 MPa. The stress path is illustrated in Fig. 3. Mineral oil was used as flooding fluid in order to avoid swelling of clay materials inside the sandstone samples.

Although the circulation pump was running the entire time during the tests, it still could take many hours before the differential pressures stabilized to permit reasonable permeability measurements. Each test series would therefore last for several days. During the overnight or over-weekend breaks, the stresses were kept constant, corresponding to creep conditions.

3. Calculations

The pressure measurements for the permeability calculations were performed when the differential pressure at the different stress conditions became stable. The permeability was then calculated using Darcys law:

$$q' = -\frac{kA}{\mu}\frac{\Delta P}{\Delta L} \tag{3}$$

$$k = -\frac{q'\mu(\Delta L)}{A(\Delta P)} \tag{4}$$

where q' is the volume rate, A is the cross section area of the core, μ is the fluid viscosity, and $\Delta P/\Delta L$ is the pressure gradient over the length L. In order to be able to estimate the accuracy of the calculated permeability, the following accuracies of the different variables were used:

Volume rate $q' \pm 2\%$
Viscosity $\mu \pm 2\%$
Core length ΔL (mid-section and total core length) $(\Delta L)_{\mathrm{mid}} \pm 0.4\%$, $(\Delta L)_{\mathrm{tot}} \pm 0.2\%$
Area $A \pm 1.1\%$
Differential pressure $\Delta P \pm 2$–3% depending on the flow rate.

All experiments were conducted at room temperature. The temperature variation was determined during a week, and the value varied within 22 ± 1 °C.

The estimated uncertainty of permeability was calculated using the formula:

$$\frac{\delta R}{R} = \sqrt{\left[\frac{\delta x}{x}\right]^2 + \left[\frac{\delta y}{y}\right]^2 + \cdots + \left[\frac{\delta z}{z}\right]^2} \tag{5}$$

where x,..., z are values of measured parameters with uncertainties δx,..., δz, and R is the calculated result

Table 5
Test results with Aalborg chalk

Sample no.	Confining pressure (MPa)	Yield stress (MPa)	*E*-modulus (GPa)	Average mid-section permeability (10^{-15} m^2)[a]	Average overall permeability (10^{-15} m^2)[a]	Permeability reduction in percent (%)	Permeability ratio[b], $k_{\text{mid-sec}}/k_{\text{overall}}$
Al1	3.0	4.7	1.4	2.99±0.12	2.29±0.10	23.5	1.30
Al4	3.0	4.7	1.6	3.11±0.12	2.98±0.12	4.0	1.04[c]
Al5	3.0	4.7	1.3	2.84±0.11	2.94±0.12	−3.5	0.96[c]
Al7	6.0	7.7	1.5	3.43±0.14	2.53±0.10	26.0	1.36

[a] Permeability uncertainties 4%.
[b] Average ratio: $k_{\text{mid-sec}}/k_{\text{overall}} = 1.17$.
[c] Permeability ratio not significant.

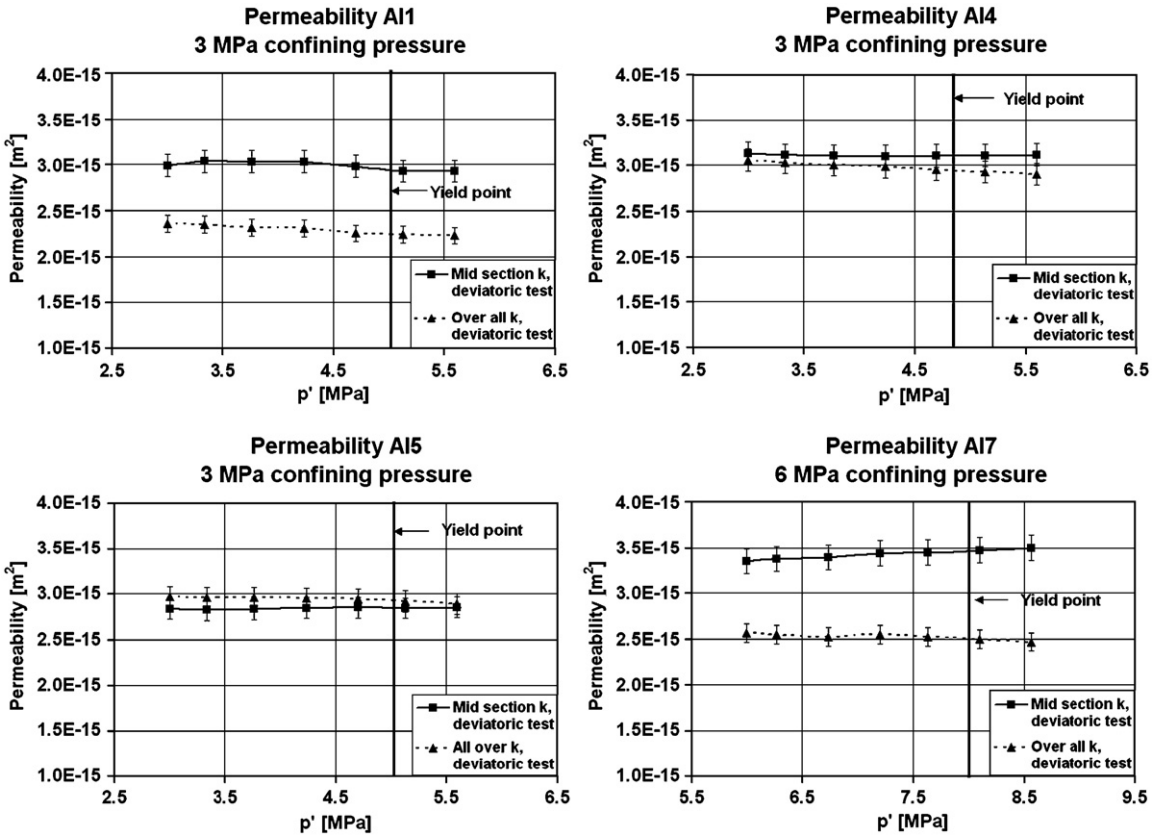

Fig. 5. Alborg chalk samples with 3 and 6 MPa confining pressure.

with uncertainty δR. The estimated uncertainty of permeability data for chalk and sandstone is ±4%.

4. Results and discussion

4.1. Chalk samples

For the chalk samples, only deviatoric tests were conducted. The effective stress was set equal to the applied stress because the typical pressure gradient when flooding the chalk cores was small (10–80 kPa), and the permeability data are presented as a function of the average effective stress, p'.

The results from the tests are plotted in stress–strain diagrams where the axial stress, σ_a, is given as a function of axial strain, ε_a. A typical diagram for the deviatoric phase is sketched in Fig. 4. In the deviatoric phase, the E-modulus is obtained directly from the slope, and the yield stress is taken as the stress level where the stress–strain curve departs substantially from approximately linear behavior. The experiments were run until the predetermined maximum axial stress level was reached.

Table 6
Test results with Liège chalk

Sample no.	Confining pressure (MPa)	Yield stress (MPa)	E-modulus (GPa)	Average mid-section permeability (10^{-15} m^2) [a]	Average overall permeability (10^{-15} m^2) [a]	Permeability reduction in percent (%)	Permeability ratio [b], $k_{mid\text{-}sec}/k_{overall}$
Li1	6.0	7.7	1.6	1.17±0.05	1.04±0.04	11.0	1.12 [c]
Li2	6.0	7.7	1.5	0.97±0.04	0.96±0.04	1.0	1.01 [c]
Li3	6.0	7.7	1.5	1.27±0.05	1.05±0.04	18.0	1.21
Li5	3.0	4.7	1.5	1.74±0.07	1.35±0.05	22.0	1.29

[a] Permeability uncertainties 4%.
[b] Average ratio: $k_{mid\text{-}sec}/k_{overall}=1.18$.
[c] Permeability ratio not significant.

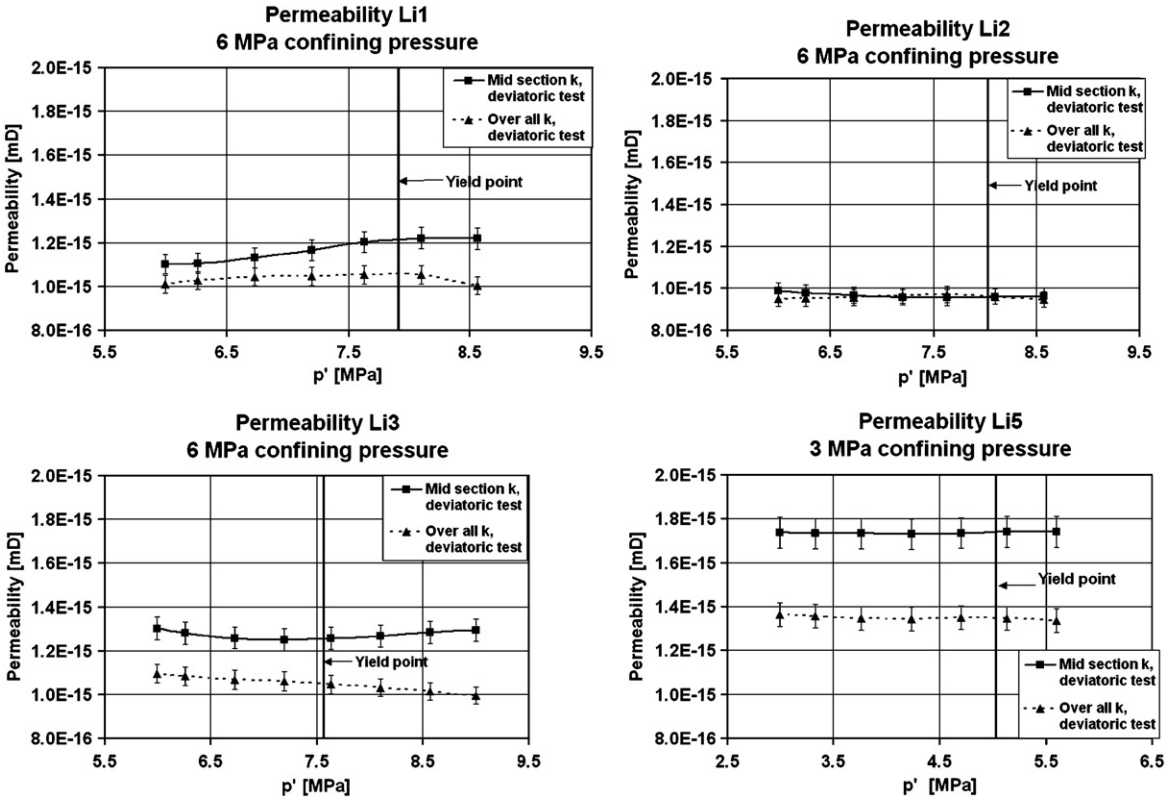

Fig. 6. Liege chalk samples with 3 and 6 MPa confining pressure.

Three tests with Aalborg chalk were run under a confining pressure of 3.0 MPa (Al1, 4, and 5), while one sample, Al7, had a confining pressure of 6.0 MPa. The mechanical data and average permeability data are presented in Table 5 and Fig. 5. As a first observation, the permeability, whether it is determined over the mid-section or the total core length, appeared to be quite constant and not affected by the increasing average effective stresses. Furthermore, for two of the cores, Al4 and Al5, no significant difference was noticed between the mid-section permeability and the overall permeability, taking into account the uncertainty in the permeability data. For the other two cores, Al1 and Al7, a significant difference in the permeability was observed. In the two cases, the mid-section permeability was a factor of 1.3 and 1.4 higher than the permeability recorded over the total core length. As expected, the yield stress point increased as the confining pressure increased from 3.0 to 6.0 MPa, i.e. from 4.7 to 7.7 MPa.

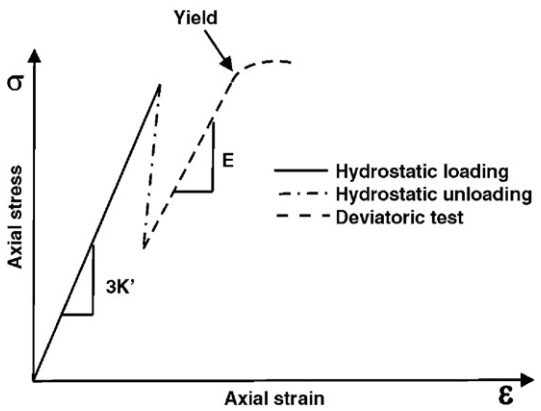

Fig. 7. Typical stress–strain plot for the sandstone cores.

In the case with Liège chalk, three of the cores were tested using 6.0 MPa as confining pressure (Li1, 2 and 3), and for the last core, Li5, the confining pressure was 3.0 MPa. The experimental results, which are presented in Table 6 and Fig. 6, are in line with the observations from Aalborg cores. This is also expected due to the similarity between the two chalk sources. Again it is observed that the permeability remained quite constant when exposed to deviatoric stresses, even beyond the yield point. At low confining pressure, Li5, the mid-section permeability value was a factor of 1.3 higher than the overall permeability determined over the total core length. Similarly, the Li3 core at 6 MPa confining pressure showed mid-section permeability that was significantly higher, a factor of 1.2,

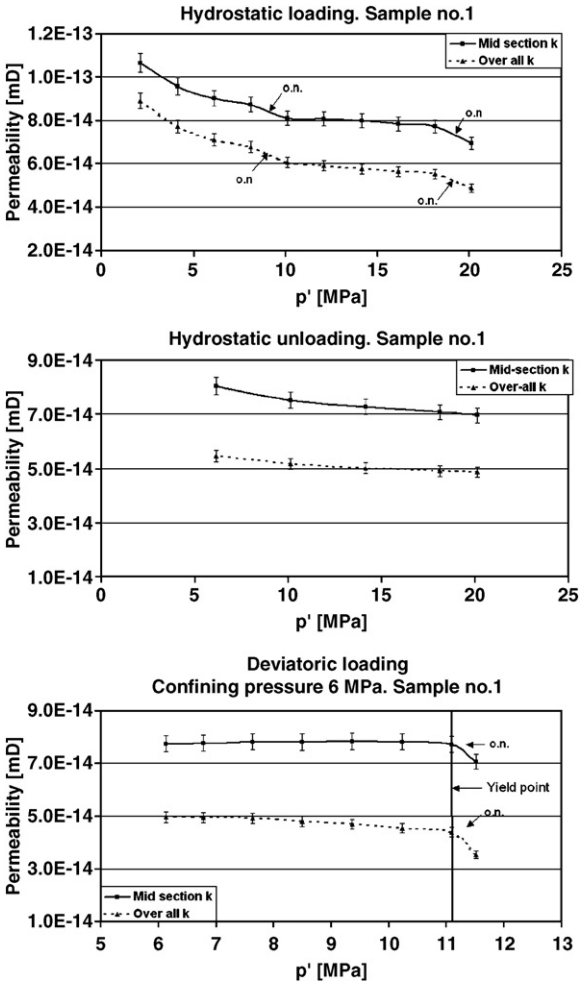

Fig. 8. Permeability vs. average effective stress plots for sandstone sample no. 1.

than the overall permeability. In the case of core Li1, there was no significant difference between the mid-section and the overall permeability for the first three axial loading steps, but for the remaining axial loading steps the mid-section permeability value is 1.2 times higher than the overall permeability. No difference in permeability was detected for the Li2 core.

For both Aalborg and Liege tests, the estimated uncertainty in the permeability (±4%) for each of the data points appeared to be somewhat higher or comparable to the variation in the permeability as the deviatoric stresses increased for the mid-section and total core length measurements. The average permeability over the mid-section and the total core was therefore calculated, and these permeability values and uncertainties are listed in Tables 5 and 6. Based on these values, the permeability ratio $k_{mid\text{-}sec}/k_{overall}$ was calculated for each of the cores. The average value of this permeability ratio for the Aaborg and Liege cores was 1.17 and 1.18, respectively, but since only 4 out of 8 samples showed significantly higher mid-section permeability than overall permeability, it cannot be concluded that end effects are playing an important role when determining permeability under deviatoric stresses for chalk. Due to the similar shape of the permeability vs. stress curves for the two cases, it is relevant to address the difference in permeability to mechanical constraints at the core ends due to physical contact with the endplates. It is also interesting to note that in most cases the gap between the mid-section and the overall permeability appears to increase slightly as the deviatoric stress increases. This is, however, not quite well documented when taking into account the uncertainties in the permeability data. The reason could be certain release of fines from the chalk materials during the experiment.

Table 7
Mechanical properties for sandstone samples

Sample no.	Loading K' (GPa)	Unloading K' (GPa)	E-modulus (GPa)	Yield stress (MPa)	Peak stress (MPa)
1	0.6	1.4	1.2	21	24
2	0.4	1.3	1.2	24	27
3	0.5	1.8	1.7	24	27

4.2. Sandstones

As can be seen from Table 4, the dry porosity values calculated based on the bulk volume and a mineral density of 2.65 g/cm^3 are always higher than the values determined by saturating the cores with mineral oil. This might be interpreted as an indication of a difference between total and effective porosity. But it might also reflect the presence of lighter substances in the "dry" state. The weight loss before saturation is an indication that there might be a residue after evaporating fluids.

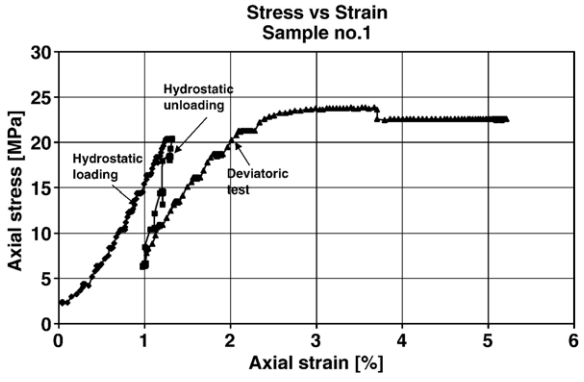

Fig. 9. Stress–strain plot for sandstone Sample no. 1.

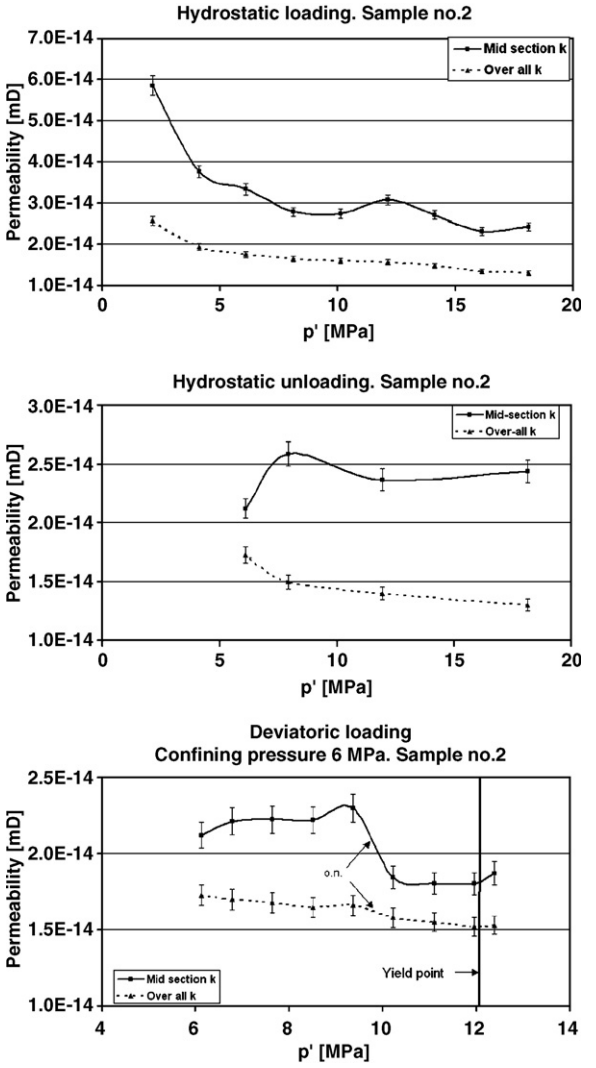

Fig. 10. Permeability vs. average effective stress plots for sandstone Sample no. 2.

To facilitate the comparison between the permeability measured in the hydrostatic and the deviatoric phases, it was decided to present the permeability data as function of the average effective stress, p'. As for the chalk samples, the average effective stress is set equal to the average applied stress because of low circulating pressure (1–10 kPa). In the deviatoric phase, the confining pressure was 6.0 MPa in all cases.

The mechanical behavior during the tests is presented in a stress–strain diagram where the axial stress is given as function of axial strain. A typical diagram is sketched in Fig. 7. From such a diagram the loading and unloading K' -module during the hydrostatic phase may be estimated. The bulk modulus K' is obtained from the actual slope divided by 3, as the volumetric strain is assumed to be 3 times the axial strain. In the deviatoric phase, the E-modulus is obtained directly from the slope, and the yield stress is taken at the stress level where the stress–strain curve departs substantially from approximately linear behavior. The experiments were run until the peak stress level for stable permeability measurements was reached. The final permeability point for each of the samples was determined at the end of the stress–strain curve.

4.2.1. Sample no. 1 (1448.85)

The permeability–average effective stress correlations are shown in Fig. 8. Both during hydrostatic loading and unloading, the mid-section permeability was significantly higher than the overall permeability. The same trend was also observed during the deviatoric phase test. The typical difference in the permeability was in the range of 20–30×10^{-15} m^2, which indicates the magnitude of the end effect in permeability measurements.

Considering details in the permeability plot, there are two steeper sections in the permeability curve during hydrostatic loading. These sections are marked with arrows and the abbreviation o.n. in order to indicate that the samples were left at constant stresses overnight. There were also overnight breaks between the hydrostatic unloading phase and the beginning of the deviatoric phase and also prior to the final permeability point at the end of the deviatoric phase. During all these breaks, the permeability is reduced, probably reflecting creep or other possible time dependent effects in the sample.

During the first part of the hydrostatic loading, there is a considerably reduction, about 30%, in permeability. But having reached an average stress level of 10 MPa, the permeability reductions became significantly smaller, maybe indicating that the stress level is approaching in-situ stresses.

The hydrostatic unloading curve shows a rather similar trend as the last part of the loading curve, indicating that

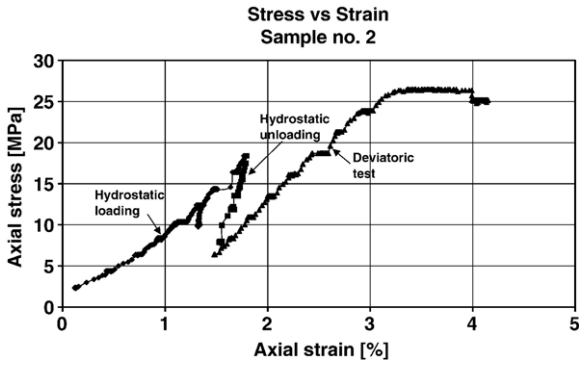

Fig. 11. Stress–strain diagram for sandstone Sample no. 2.

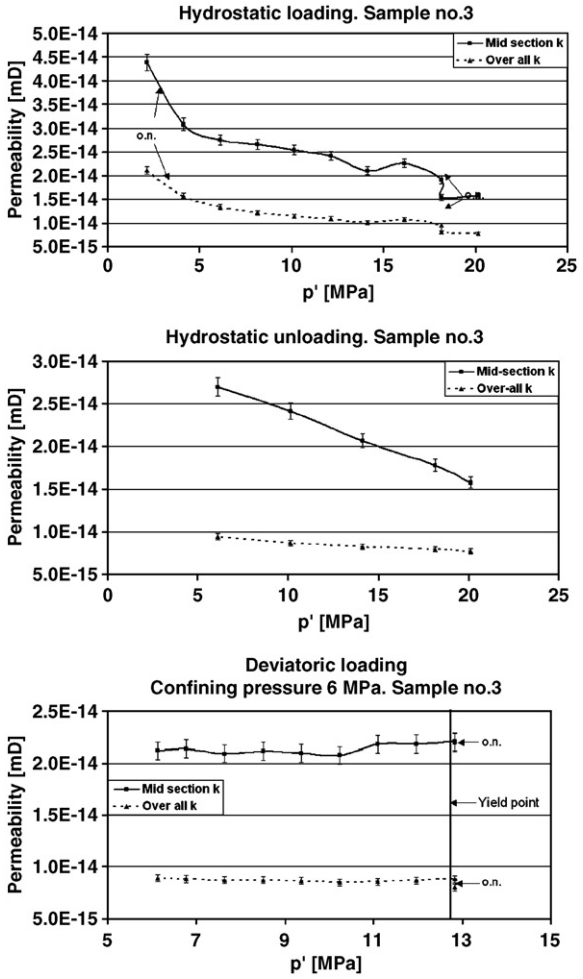

Fig. 12. Permeability vs. average effective stress plots for sandstone Sample no. 3.

apart from creep or time effects, the permeability changes are largely reversible before reaching yield stress. At the last hydrostatic unloading step, $p'=6$ MPa, the mid-section permeability was 8.0×10^{-14} m^2 compared to 9.0×10^{-14} m^2 at the same hydrostatic loading step. The value for the overall permeability was 5.5×10^{-14} m^2 at the last hydrostatic unloading step instead of 7.1×10^{-14} m^2 at the same hydrostatic loading step.

In the deviatoric phase, the mid-section and the overall permeability remained almost constant below the yield point. The sudden decrease in permeability above the yield point is most probably related to certain creep effects when the system was left overnight at constant stress. The mechanical properties listed in Table 7 were calculated from the stress–strain curve presented in Fig. 9. The final stress level was slightly reduced in order to achieve stabilized permeability measurements.

4.2.2. Sample no. 2 (1448.95A)

The permeability data are presented in Fig. 10. During the hydrostatic unloading phase, a leak was detected, and the test had to be stopped right after a stress level of 8 MPa. After having remounted the sample, the deviatoric phase was run. However, the trend in the permeability–average effective stress curves were quite similar to what was observed for Sample no. 1. In general, the permeability difference between the mid-section and the overall permeability was somewhat lower than for Sample no. 1, i.e., in the range of 5–10×10^{-15} m^2. Another striking feature is that the permeability is about a factor of 3 lower than for Sample no. 1, even though the samples were taken only 10 cm lower in the reservoir, Table 3. The two samples are, however, sampled in different directions, i.e. Sample no. 1 is sampled horizontally while Sample no. 2 is taken vertically. It is well known that the vertical permeability is lower than the horizontal permeability due to the packing of the grains in sandstones. This may also reflect the difference in the gap between the mid-section and overall permeabilities observed for the two samples.

The mechanical data listed in Table 7 were determined from the stress–strain plot shown in Fig. 11. Again, the final stress level was slightly reduced in order to achieve stabilized permeability measurements.

4.2.3. Sample no. 3 (1448.95B)

Sample nos. 2 and 3 should be very comparable in properties because both of the samples were taken at the same depth and in the vertical direction, Table 3. The permeability–average effective stress curves for Sample no. 3 are presented in Fig. 12. The striking difference is the strong increase in the mid-section permeability during the hydrostatic unloading, which leads to a larger gap between the mid-section and overall permeability during the deviatoric phase. Otherwise, the permeability behavior was quite similar to the previous sandstone samples.

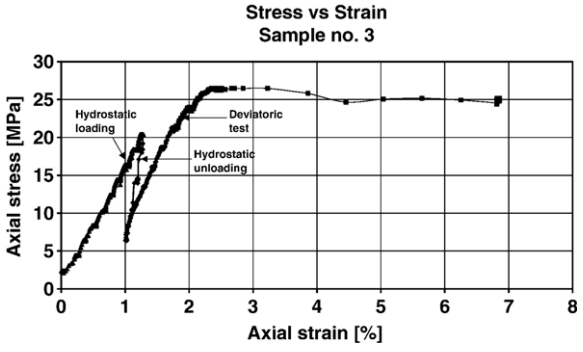

Fig. 13. Stress–strain diagram for sandstone Sample no. 3.

The hydrostatic loading phase started with an overnight break after the first permeability measurement. Still the permeability reduction during this break is rather similar to what was observed for Sample no. 2. Another overnight break was made towards the end of the loading section. Therefore, it is difficult to compare the results from Sample nos. 2 and 3, because the cores have been subjected to different creep periods. The mechanical data listed in Table 7 were determined from the stress–strain plot shown in Fig. 13.

During the deviatoric phase, there was a major breakdown of the sample after the penultimate permeability measurement. The axial strain as function of time after the penultimate permeability point (creep phase) is presented in Fig. 14. A little more than 200 min after the penultimate permeability measurement, there was a steadily increase in axial strain, until the piston stopped because the moving limit for the piston was reached. When studying the core afterwards, it was noticed that a major part of the sample was more or less crushed in shear failure. Fig. 12 shows however that there was almost no reaction in mid-section and overall permeability after the sample breakdown.

5. Concluding summary

5.1. Chalk

The mechanical properties of the chalk samples are shown in Tables 5 and 6. Chalk from Aalborg and Liège has the same yield point when tested at equal confining pressures, and the *E*-moduli are fairly constant between 1.3 GPa and 1.6 GPa for all the samples.

The permeability ratio between the mid-section and the overall permeability varies from 1.0 to 1.4, Tables 5 and 6, but only half of the samples showed a mid-section permeability value 1.2 to 1.4 times higher than the overall permeability value. Three of the samples showed a permeability ratio of 1.0 between mid-section

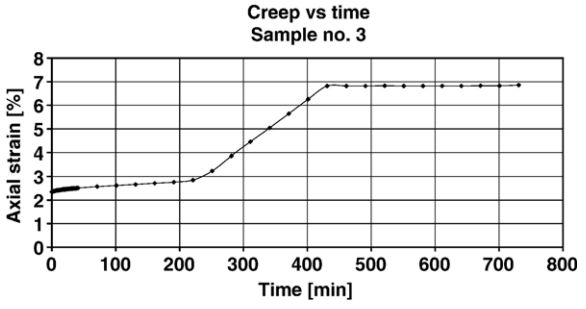

Fig. 14. Creep behavior for sandstone Sample no. 3.

Fig. 15. SEM picture of chalk.

permeability and overall permeability. The last chalk sample, Li1, show no significant difference in mid-section permeability and overall permeability during the first three axial loading steps, but the remaining loading steps showed a mid-section permeability value 1.2 times higher than the overall permeability value. Generally it can therefore not be concluded that end effects play a significant role when the chalk cores undergo a deviatoric test. The scattering in the data may be related to the properties of the chalk material, which is mainly built up of whole and fragmentary parts of calcite skeletons produced by planktonic algae, known as coccolithophorids. At grain size level, this build-up of whole and fragmentary calcite parts makes the chalk a highly inhomogeneous material, as illustrated by the scanning electron microscope (SEM) photo shown in Fig. 15, and this can cause certain variations in chalk properties even between samples that were prepared from the same block. Mechanically, high porosity chalks behave as frictional materials, failing in a shear failure mode (Risnes and Kristensen, 1996).

The measured permeability values for both Aalborg and Liège chalk were in the range of what is expected for these two types of chalk, Liège chalk around $1–2\times10^{-15}$ m^2 and Aalborg around $2–3\times10^{-15}$ m^2, as shown in Table 1. In the deviatoric tests the increasing stress is applied parallel to the flow direction, and the change in the permeability is very small, nearly within the uncertainty for both the mid-section and the overall permeabilities. This observation is in line with previously published data on weakly cemented sandstones. Bruno et al. (1991) showed that the permeability reduction was relatively small when the stress was applied parallel to the flow direction, but the same stress magnitude was much more significant when applied perpendicular to the direction of flow.

Table 8
Permeability ratio between $k_{\text{mid-section}}$ and k_{overall}

Sample no.	Mid-section permeability (10^{-15} m^2) [a]	Overall permeability (10^{-15} m^2) [a]	Permeability ratio, $k_{\text{mid}}/k_{\text{overall}}$
1	70±3 [b] (78±3) [c]	48±2 [b] (50±2) [c]	1.4 [b] (1.6) [c]
2	24±1 (21.2±0.9)	12.8±0.5 (17.8±0.7)	1.9 (1.2)
3	15.8±0.6 (21.2±)	7.9±0.3 (8.9±0.4)	2.0 (2.4)

[a] Permeability uncertainties 4%.
[b] Permeability at the end of the hydrostatic phase, i.e. at 20 MPa.
[c] Permeability at the start of the deviatoric phase.

The permeability measurements with Aalborg and Liège chalk cannot conclude end effects, but the results indicate that measurements from the mid-section and the entire core length have a similar permeability pattern with increasing average stress. The permeability response due to increasing axial stress seem not to be much affected whether the permeability is measured over the mid-section or the entire core length.

5.2. Sandstone

The mechanical properties of the sandstone samples are summarized in Table 7. The values show a rather consistent picture. It is, however, interesting to note that yield stress and peak stress is similar for the two cores, which were sampled vertically, while the values are slightly smaller for the core sampled horizontally.

To compare the permeability between the different plugs, the stress conditions and the stress path followed should be the same (Bruno et al., 1991). The permeability values at the end of the hydrostatic phase, i.e. at 20 MPa, are compiled in Table 8. Also the permeability values at the start of the deviatoric phase are given in parenthesis. The gap between the permeability determined over the mid-section and over the total core lengths was a factor between 1.2 and 2.4. For the two sandstone cores sampled vertically, i.e. Sample nos. 2 and 3, the permeability ratio at the end of the hydrostatic phase was a factor 2, which points to strong end effects. For the core sampled horizontally, the permeability ratio was smaller, 1.4. The reason for such a strong end effect for the sandstone cores is not clear. If this is related to the release of fines, which are collected on the filter paper at the end of the core to cause a larger pressure gradient, the difference in permeability between the mid-section and the overall permeability should increase with time, but this is not the case.

During the hydrostatic test, the permeability decreased as the average effective stress increased. The permeability during the deviatoric test remained quite constant, which is in line with the results from the chalk samples and previous published work, as discussed previously (Bruno et al., 1991).

The results indicate that end effects do not alter the response of permeability due to increasing hydrostatic and deviatoric stresses. The permeability measurements from the mid-section and the entire core length show approximately the same permeability pattern with increasing average stress.

Without mechanical deformation at the core ends, and having flow condition without capillary forces (one phase flow), small differences between mid-section permeability and overall permeability is expected. The observed end effects for the sandstone samples are therefore most likely induced from the stresses between the axial steel pistons and the sample ends.

Nomenclature

A	cross-sectional area of sample, mm^2
E	Young's modulus, GPa
K	constant stress ratio test
K'	bulk modulus, GPa
k	permeability, m^2
$(\Delta L)_{\text{mid}}$	mid-section core length, mm
$(\Delta L)_{\text{tot}}$	total core length, mm
ΔP	differential pressure, kPa
p'	average effective stress, MPa
q	generalized shear stress, MPa
q'	volume rate, ml/min
ε_a	axial strain, %
μ	viscosity, Pa s
σ'	effective axial stress, MPa
σ_a	axial stress, MPa

Acknowledgement

The authors wish to thank The Research Council of Norway and the Ekofisk Licence for a dr. grant for R. I. Korsnes.

References

Bruno, M., Bovberg, C., Nakagaw, F., 1991. Anisotropic influence on the permeability of weakly cemented sandstone. Paper Presented at the 32nd U.S. Symposium on Rock Mechanics, Norman, OK, July 10–12, pp. 375–383.

David, C., Wong, T.F., Zhu, W., Zhang, J., 1994. Laboratory measurement of compaction-induced permeability change in porous rocks: implications for the generation and maintenance of pore pressure excess in the crust. PAGEOPH 143, 425–456.

Da-Silva, F., Sarda, J.P., Schroeder, C., 1985. Mechanical behaviour of chalk. Second North Sea Chalk Symposium, Stavanger, Norway.

Holt, R.M., 1989. Permeability reduction induced by a nonhydrostatic stress field. Paper SPE19595 Presented at 64th Annual Technical Conference, Soc. of Pet. Eng., San Antonio, pp. 444–448.

Rhett, D.W., Teufel, L.W., 1992. Effect of reservoir stress path on compressibility and permeability of sandstones. Paper SPE24756 Presented at 67th Annual Technical Conference, Soc. of Pet. Eng., Washington, pp. 965–972.

Risnes, R., 2001. Deformation and yield in high porosity outcrop chalk. Phys. Chem. Earth (A) 26 (1–2), 53–57.

Risnes, R., Kristensen, C.N., 1996. Triaxial tests on high porosity chalk with different saturating fluids. Fifth North Sea Chalk Symposium, Reims, France.

Teufel, L.W., Warpinski, N.R., 1990. Laboratory determination of effective stress laws for deformation and permeability of chalk. Third North Sea Chalk Symposium, Copenhagen, Denmark.

Teufel, L.W., Rhett, D.W., 1992. Effect of reservoir stress path on permeability of fractures in chalk. Fourth North Sea Chalk Symposium, Deaville, France.

Zhu, W., Wong, T.F., 1997. The transition from brittle faulting to cataclastic flow: permeability evolution. J. Geophys. Res. 102, 3027–3041.